Supporting Information

A family of doped lanthanide metal-organic frameworks for wide-range temperature sensing and tunable white light emission

Yan Yang,[a,b] Lian Chen,*[a] Feilong Jiang,[a] Muxin Yu,[a,b] Xiuyan Wan,[a] Bo Zhang,[a,b] and Maochun Hong*[a]

[a]*State Key Laboratory of Structure Chemistry, Fujian Institute of Research on the Structure of Matter, Chinese Academy of Sciences, Fuzhou 350002, China.*
[b]*University of the Chinese Academy of Sciences, Beijing, 10049, China*

Contents

$Eu_{0.0089}Tb_{0.9911}L$ at different temperatures from 77 to 450 K. (d) CIE-1931 chromaticity diagram showing the luminescent colors of the binary mixed **$Eu_{0.0089}Tb_{0.9911}L$**.

Fig. S17 (a) Solid-state emission spectra of **$Eu_{0.033}Tb_{0.085}Gd_{0.882}L$** recorded between 77 K and 450 K excited at 335 nm. (b) Temperature-dependent normalized emission intensity of the $^5D_4 \rightarrow {}^7F_5$ and $^5D_0 \rightarrow {}^7F_2$ transitions of **$Eu_{0.033}Tb_{0.085}Gd_{0.882}L$**. (c) Temperature-dependent intensity ratio of Tb^{3+} (542 nm) to Eu^{3+} (612 nm) for ternary mixed **$Eu_{0.033}Tb_{0.085}Gd_{0.882}L$** at different temperatures from 77 to 450 K. (b) CIE-1931 chromaticity diagram showing the luminescent colors of the ternary mixed **$Eu_{0.033}Tb_{0.085}Gd_{0.882}L$**.

Fig. S18 Comparison of the temperature-dependent intensity ratio (I_{Tb}/I_{Eu}) of **$Eu_{0.0089}Tb_{0.9911}L$**, **$Eu_{0.0066}Tb_{0.9934}L$**, **$Eu_{0.013}Tb_{0.060}Gd_{0.927}L$**, **$Eu_{0.033}Tb_{0.085}Gd_{0.882}L$** and temperature-dependent intensity of Tb^{3+} (542 nm) for **TbL**.

Fig. S19 The relative thermometric sensitivity values for mixed LnMOFs **$Eu_{0.0089}Tb_{0.9911}L$**, **$Eu_{0.0066}Tb_{0.9934}L$**, **$Eu_{0.013}Tb_{0.060}Gd_{0.927}L$** and **$Eu_{0.033}Tb_{0.085}Gd_{0.882}L$** determined from the curves plotting of I_{Tb}/I_{Eu} *vs.* temperature.

Fig. S20 Temperature-dependent lifetimes of the $^5D_0 \rightarrow {}^7F_2$ transitions (612 nm) and $^5D_4 \rightarrow {}^7F_5$ transitions (542 nm) for the ternary mixed (a) **$Eu_{0.013}Tb_{0.060}Gd_{0.882}L$** and (b) **$Eu_{0.033}Tb_{0.085}Gd_{0.882}L$** between 77 K and 450 K excited at 335 nm.

Scheme S1. Simplified schematic diagram of the ligand–metal energy transfer in the ternary mixed lanthanide MOFs, **$Eu_{0.013}Tb_{0.060}Gd_{0.882}L$** and **$Eu_{0.033}Tb_{0.085}Gd_{0.882}L$**

Fig. S21 Solid-state emission spectrum of the **$Eu_{0.0062}Tb_{0.0087}Gd_{0.9851}L$** at room temperature excited at 335 nm.

Fig. S22 Solid-state emission spectrum of the **$Eu_{0.0062}Tb_{0.0087}Gd_{0.9851}L$** at room temperature excited at (a) 350 nm, (b) 355 nm, (c) 360 nm, (d) 365 nm, (e) 370 nm, (f) 375 nm.

Table S1. The original ratios of different lanthanide metal salts and the corresponding ICP results.

Table S2. The parameters containing composition, temperature ranges (K), maximum relative sensitivity values (S_m, % K^{-1}), the temperature at which S_m is maximum (T_m, K) of several selected ratiometric luminescent MOF thermometers.

Table S3. Crystal data and refinement results for **EuL**, **GdL** and **TbL**.

Table S4. Selected bond lengths (Å) and bond angles (º) for **EuL**, **GdL** and **TbL**.

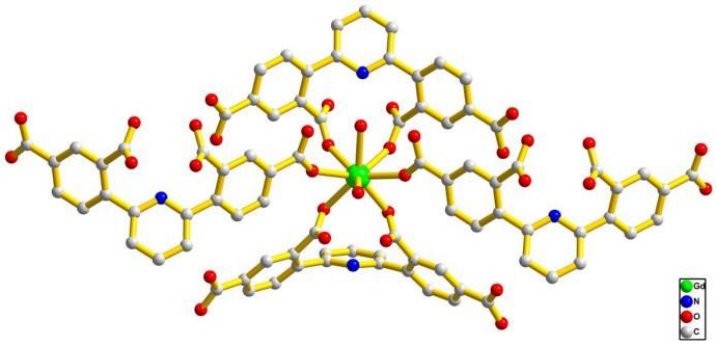

Fig. S1 The coordinated environment of Gd^{3+} ion in compound **GdL**.

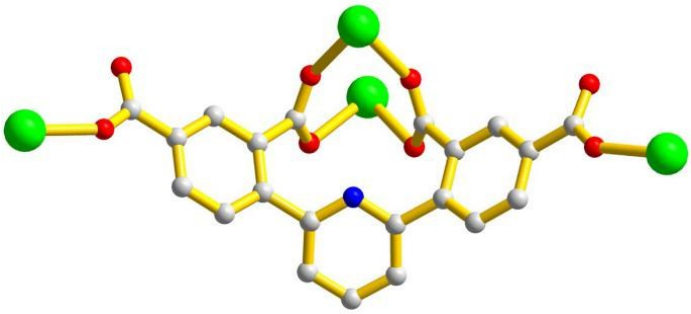

Fig. S2 The coordination mode of $[L]^{4-}$ in **GdL**: μ_4-bridging mode.

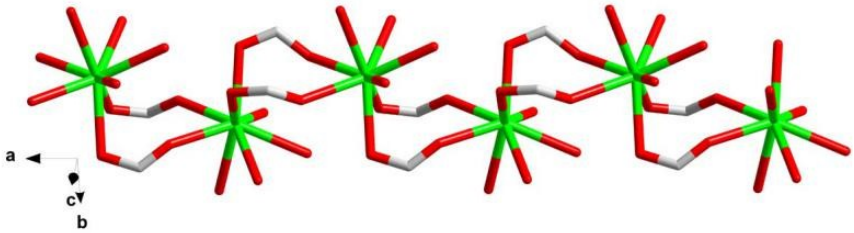

Fig. S3 1D metal-chain $[Gd_2(\mu_2\text{-}COO)_2]_n$ in **GdL**.

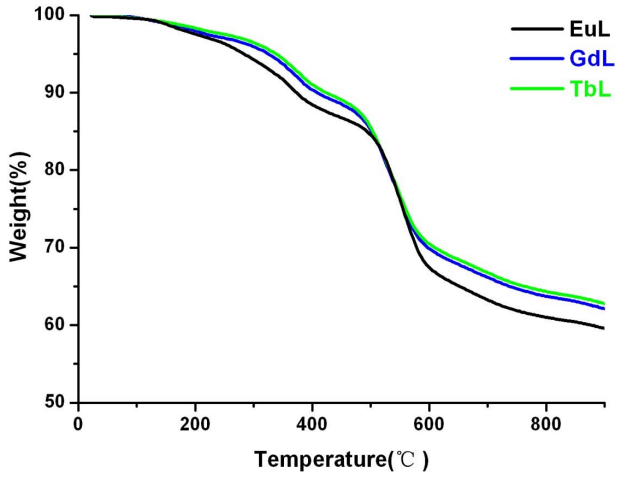

Fig. S4 TGA curve of **EuL**, **GdL** and **TbL**.

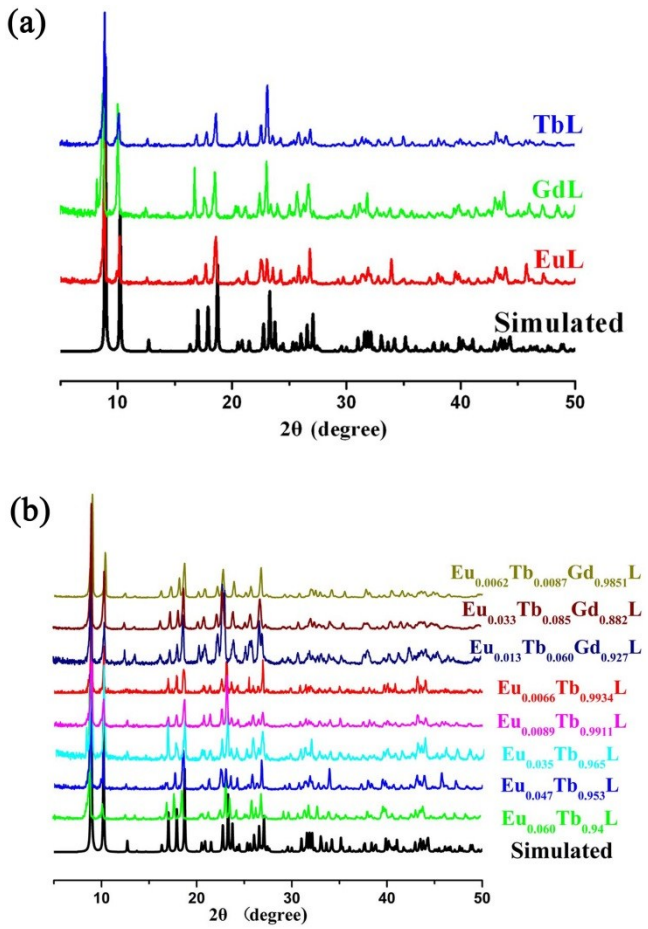

Fig. S5 (a) PXRD patterns of the as-synthesized **EuL** (red), **GdL** (green) and **TbL** (blue). (b) PXRD patterns of all the mixed $\mathbf{Eu_xTb_{1-x}L}$ and $\mathbf{Eu_xTb_yGd_{1-x-y}L}$.

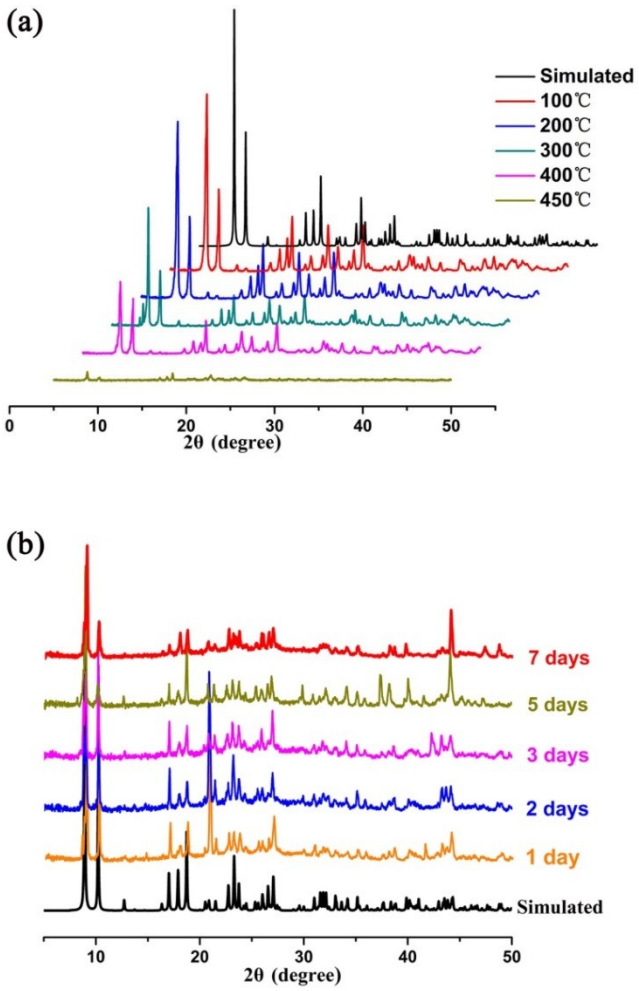

Fig. S6 (a) The X-ray thermodiffractogram of **GdL**. (b) PXRD patterns of **GdL** after exposed to open air containing H_2O vapor for 1 day, 2 days, 3 days, 5 days and 7 days.

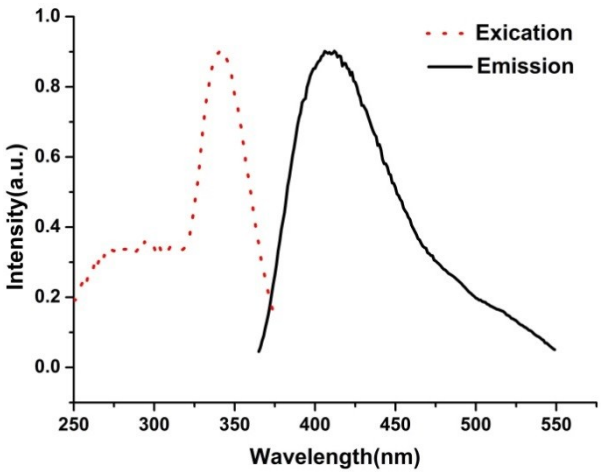

Fig. S7 Solid-state luminescent spectra of the ligand H_4L (excitation: dot, λ_{em}= 412 nm; emission: solid, λ_{ex}= 341 nm) at room temperature.

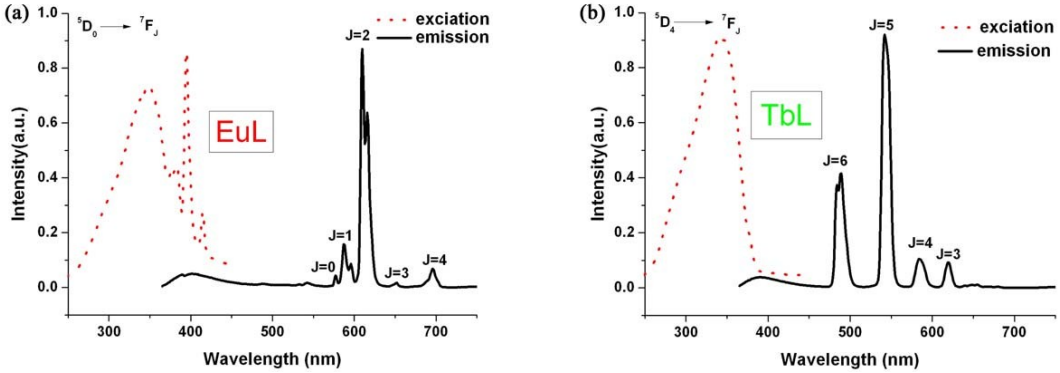

Fig. S8 Solid-state luminescent spectra of (a) **EuL** (excitation: dot, λ_{em}= 612 nm; emission: solid, λ_{ex}= 335 nm) and (b) **TbL** (excitation: dot, λ_{em}= 542 nm; emission: solid, λ_{ex}= 335 nm) at room temperature.

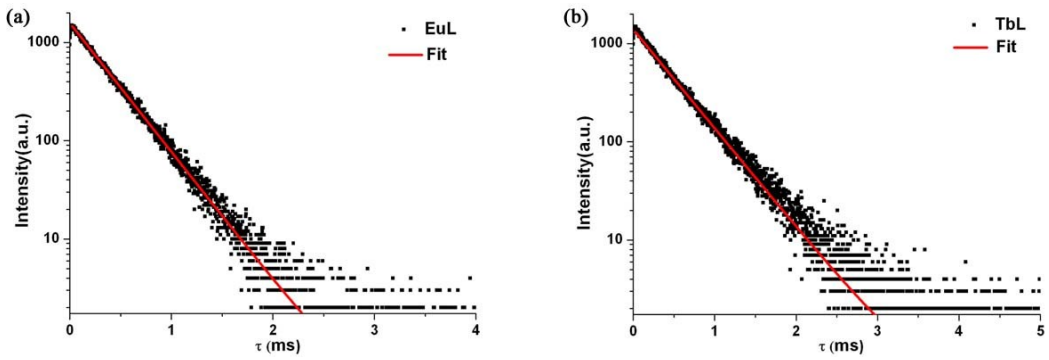

Fig. S9 The luminescence decay curves for (a) **EuL** by monitoring the $^5D_0 \rightarrow {}^7F_2$ transition (612 nm) excited at 335 nm and (b) **TbL** by monitoring the $^5D_4 \rightarrow {}^7F_5$ transition (542 nm) excited at 335 nm at room temperature. The scattering points are the experimental data and the solid lines are the fitting results.

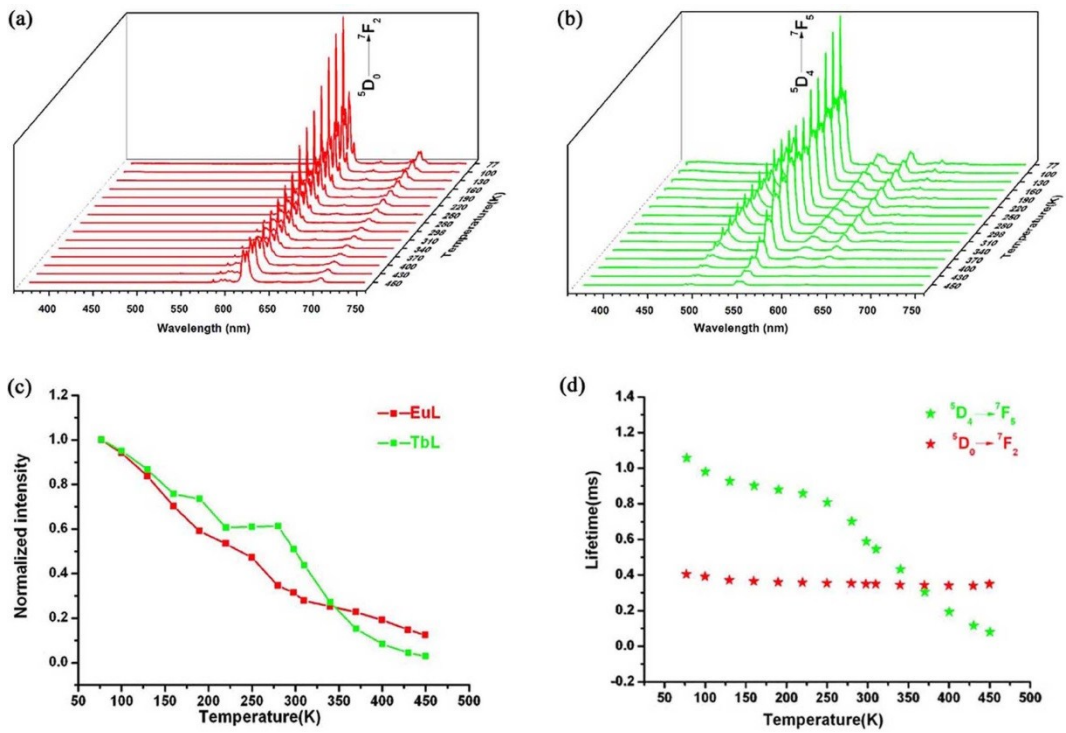

Fig. S10 Solid-state emission spectra of (a) **EuL** and (b) **TbL** recorded between 77 K and 450 K excited at 335 nm. (c) Temperature-dependent normalized emission intensity of the $^5D_0 \rightarrow {}^7F_2$ transitions (612 nm) for **EuL** and $^5D_4 \rightarrow {}^7F_5$ transitions (542 nm) for **TbL**. (d) Temperature-dependent lifetimes of the $^5D_0 \rightarrow {}^7F_2$ transitions (612 nm) for **EuL** and $^5D_4 \rightarrow {}^7F_5$ transitions (542 nm) for **TbL** excited at 335 nm.

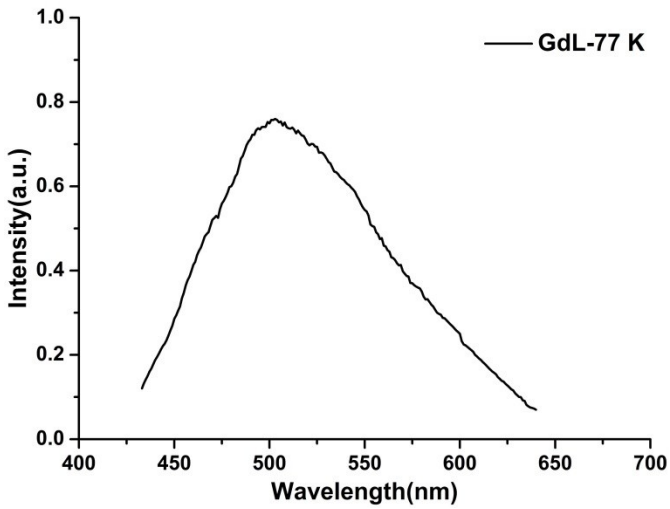

Fig. S11 The phosphorescence spectra of compound $[Me_2NH_2][GdL(H_2O)_2]$ (**GdL**) at 77 K. The ligand-centered triplet state T_1 was calculated from the shortest wavelength emission edge of the phosphorescence spectrum of compound $[Me_2NH_2][GdL(H_2O)_2]$

(**GdL**) at 77 K. The phosphorescence spectrum of **GdL** reveals that the triplet state energy level T_1 of the ligand is 23753 cm^{-1} (421 nm).

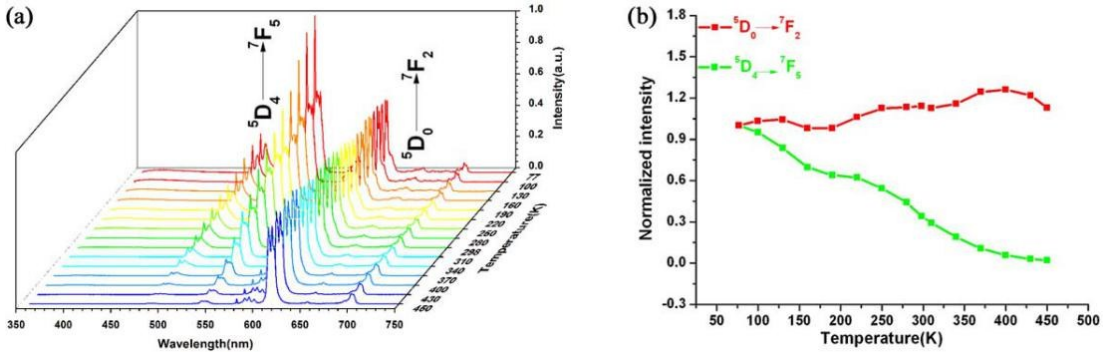

Fig. S12 (a) Solid-state emission spectra of $\mathbf{Eu_{0.060}Tb_{0.94}L}$ recorded between 77 K and 450 K excited at 335 nm. (b) Temperature-dependent normalized emission intensity of the $^5D_4 \rightarrow {}^7F_5$ and $^5D_0 \rightarrow {}^7F_2$ transitions of $\mathbf{Eu_{0.060}Tb_{0.94}L}$.

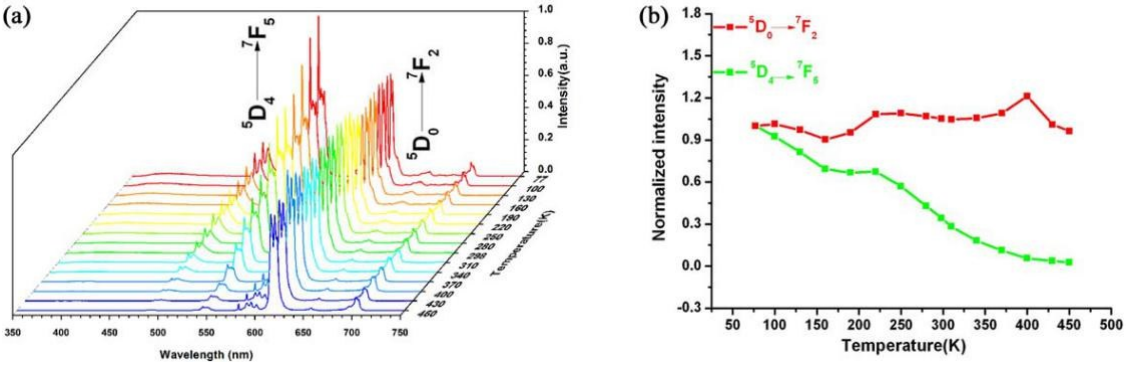

Fig. S13 (a) Solid-state emission spectra of $\mathbf{Eu_{0.047}Tb_{0.953}L}$ recorded between 77 K and 450 K excited at 335 nm. (b) Temperature-dependent normalized emission intensity of the $^5D_4 \rightarrow {}^7F_5$ and $^5D_0 \rightarrow {}^7F_2$ transitions of $\mathbf{Eu_{0.047}Tb_{0.953}L}$.

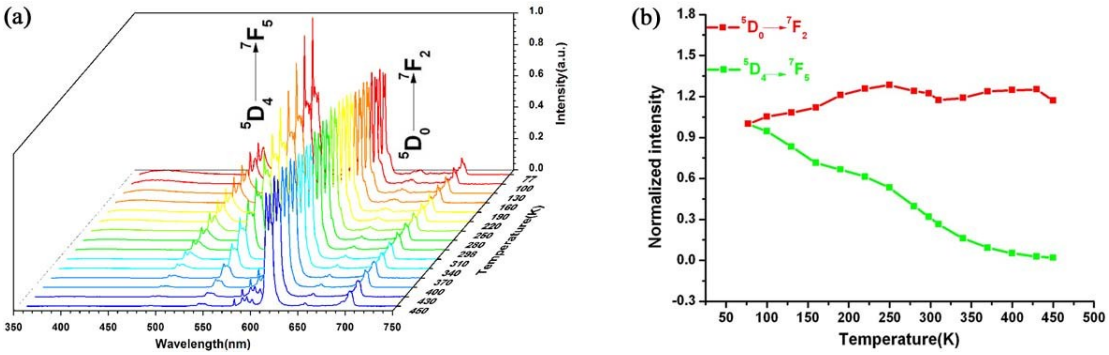

Fig. S14 (a) Solid-state emission spectra of $\mathbf{Eu_{0.035}Tb_{0.965}L}$ recorded between 77 K and

450 K excited at 335 nm. (b) Temperature-dependent normalized emission intensity of the $^5D_4 \rightarrow {}^7F_5$ and $^5D_0 \rightarrow {}^7F_2$ transitions of $\mathbf{Eu_{0.035}Tb_{0.965}L}$.

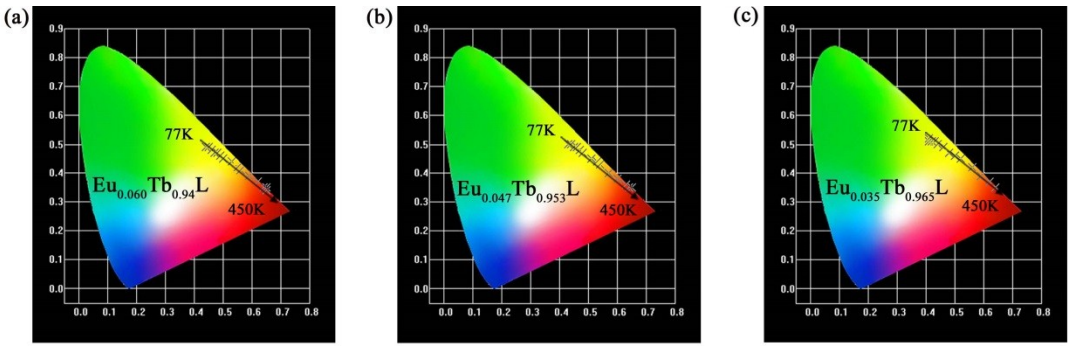

Fig. S15 CIE-1931 chromaticity diagram showing the luminescent colors of the binary mixed $\mathbf{Eu_xTb_yL}$ (x=0.060, 0.047, 0.035, 0.0066) at different temperatures from 77 K to 450 K.

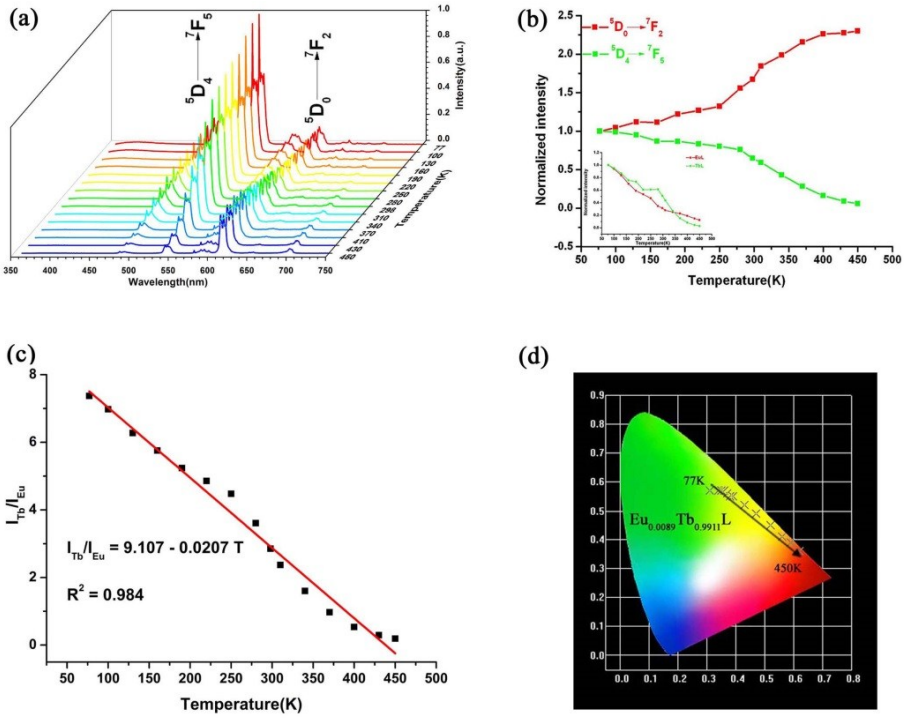

Fig. S16 (a) Solid-state emission spectra of $\mathbf{Eu_{0.0089}Tb_{0.9911}L}$ recorded between 77 K and 450 K excited at 335 nm. (b) Temperature-dependent normalized emission intensity of the $^5D_4 \rightarrow {}^7F_5$ and $^5D_0 \rightarrow {}^7F_2$ transitions of $\mathbf{Eu_{0.0089}Tb_{0.9911}L}$. (c) Temperature-dependent intensity ratio of Tb^{3+} (542 nm) to Eu^{3+} (612 nm) for binary mixed $\mathbf{Eu_{0.0089}Tb_{0.9911}L}$ at different temperatures from 77 to 450 K. (d) CIE-1931 chromaticity

diagram showing the luminescent colors of the binary mixed **$Eu_{0.0089}Tb_{0.9911}L$**.

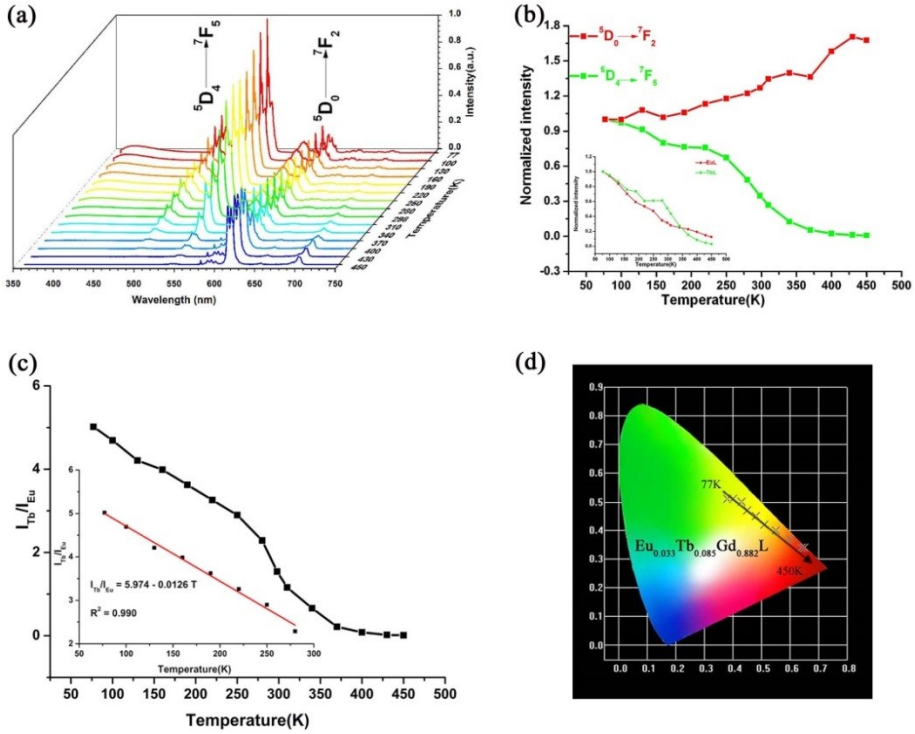

Fig. S17 (a) Solid-state emission spectra of **$Eu_{0.033}Tb_{0.085}Gd_{0.882}L$** recorded between 77 K and 450 K excited at 335 nm. (b) Temperature-dependent normalized emission intensity of the $^5D_4 \rightarrow {}^7F_5$ and $^5D_0 \rightarrow {}^7F_2$ transitions of **$Eu_{0.033}Tb_{0.085}Gd_{0.882}L$**. (c) Temperature-dependent intensity ratio of Tb^{3+} (542 nm) to Eu^{3+} (612 nm) for ternary mixed **$Eu_{0.033}Tb_{0.085}Gd_{0.882}L$** at different temperatures from 77 to 450 K. (d) CIE-1931 chromaticity diagram showing the luminescent colors of the ternary mixed **$Eu_{0.033}Tb_{0.085}Gd_{0.882}L$**.

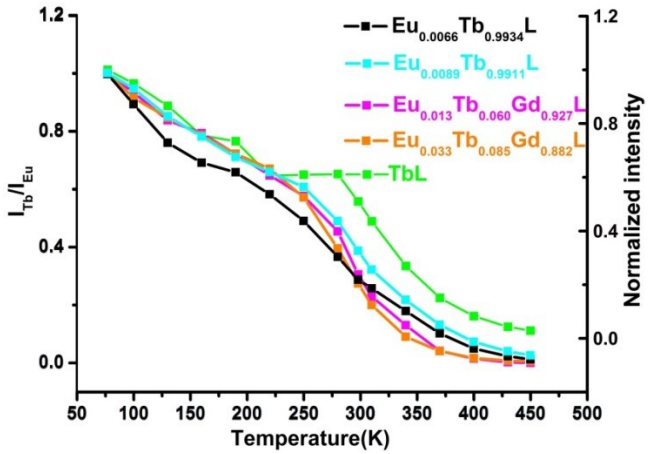

Fig. S18 Comparison of the temperature-dependent intensity ratio (I_{Tb}/I_{Eu}) of **$Eu_{0.0089}Tb_{0.9911}L$**, **$Eu_{0.0066}Tb_{0.9934}L$**, **$Eu_{0.013}Tb_{0.060}Gd_{0.927}L$**, **$Eu_{0.033}Tb_{0.085}Gd_{0.882}L$** and temperature-dependent intensity of Tb^{3+} (542 nm) for **TbL**.

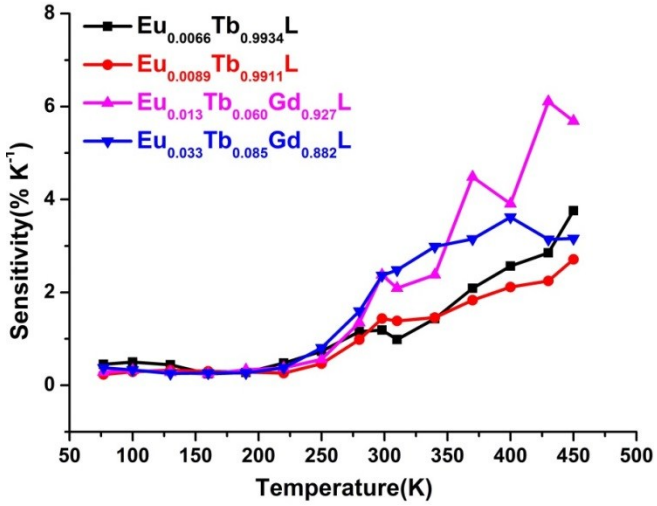

Fig. S19 The relative thermometric sensitivity values for mixed LnMOFs **$Eu_{0.0089}Tb_{0.9911}L$**, **$Eu_{0.0066}Tb_{0.9934}L$**, **$Eu_{0.013}Tb_{0.060}Gd_{0.927}L$** and **$Eu_{0.033}Tb_{0.085}Gd_{0.882}L$** determined from the curves plotting of I_{Tb}/I_{Eu} *vs.* temperature.

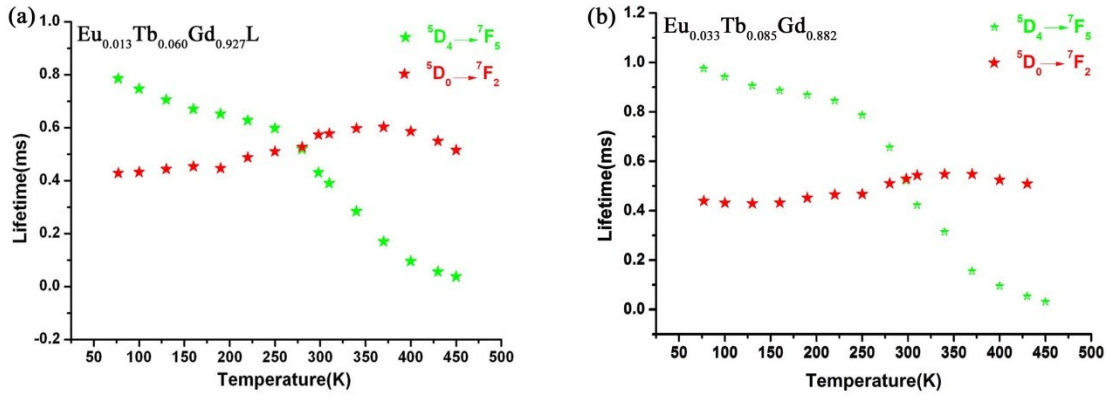

Fig. S20 Temperature-dependent lifetimes of the $^5D_0 \rightarrow {}^7F_2$ transitions (612 nm) and $^5D_4 \rightarrow {}^7F_5$ transitions (542 nm) for the ternary mixed (a) $\mathbf{Eu_{0.013}Tb_{0.060}Gd_{0.882}L}$ and (b) $\mathbf{Eu_{0.033}Tb_{0.085}Gd_{0.882}L}$ between 77 K and 450 K excited at 335 nm.

Scheme S1. Simplified schematic diagram of the ligand–metal energy transfer in the ternary mixed lanthanide MOFs (S_0 is the ground state of the ligand; S_1 and T_1 are the singlet state and triplet state of the ligand, respectively.).

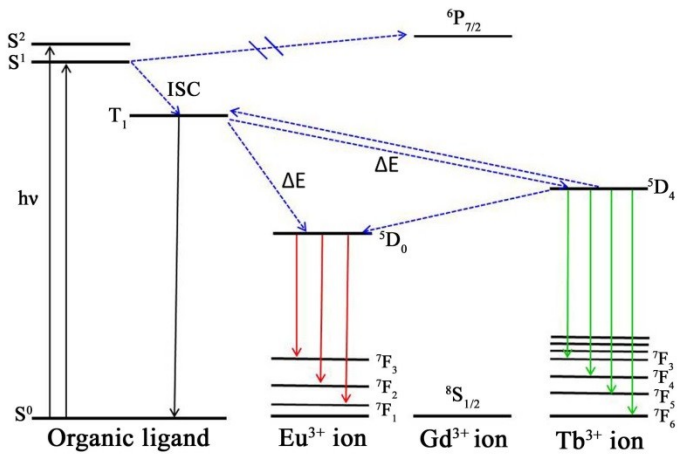

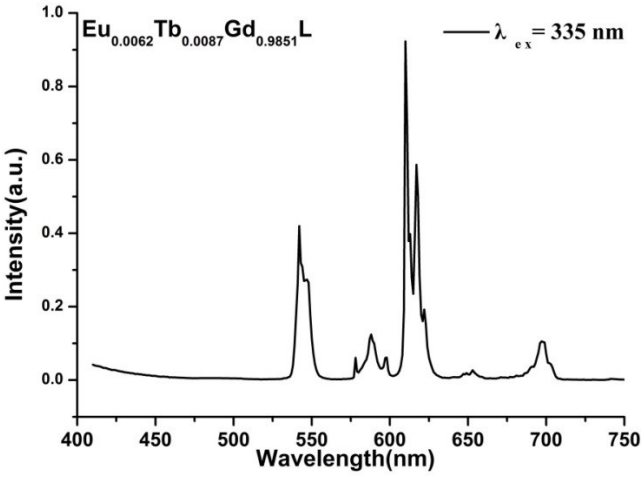

Fig. S21 Solid-state emission spectrum of the $\mathbf{Eu_{0.0062}Tb_{0.0087}Gd_{0.9851}L}$ at room temperature excited at 335 nm.

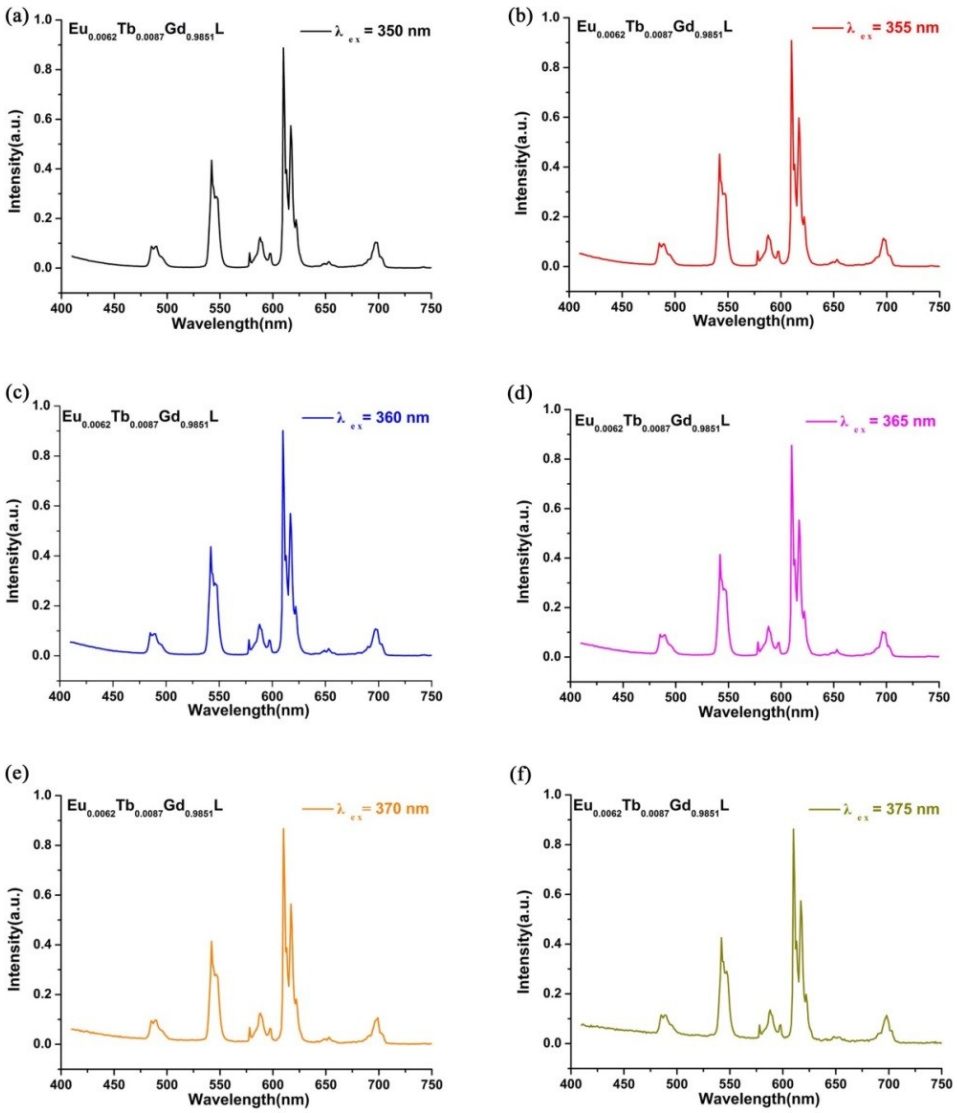

Fig. S22 Solid-state emission spectra of the $\mathbf{Eu_{0.0062}Tb_{0.0087}Gd_{0.9851}L}$ at room temperature excited at (a) 350 nm, (b) 355 nm, (c) 360 nm, (d) 365 nm, (e) 370 nm, (f) 375 nm.

Table S1. The original ratios of different lanthanide metal salts and the corresponding ICP results.

	Experimental			**ICP Results**		
$\mathbf{Eu_xTb_yL}$	Eu(x)		Tb(y)	Eu(x)		Tb(y)
$\mathbf{Eu_{0.060}Tb_{0.94}L}$	0.1		0.9	0.060		0.94
$\mathbf{Eu_{0.047}Tb_{0.953}L}$	0.08		0.92	0.047		0.953
$\mathbf{Eu_{0.035}Tb_{0.965}L}$	0.05		0.95	0.035		0.965
$\mathbf{Eu_{0.0089}Tb_{0.9911}L}$	0.02		0.98	0.0089		0.9911
$\mathbf{Eu_{0.0066}Tb_{0.9934}L}$	0.01		0.99	0.0066		0.9934
$\mathbf{Eu_xTb_yGd_{1\text{-}x\text{-}y}L}$	Eu(x)	Tb(y)	Gd(1-x-y)	Eu(x)	Tb(y)	Gd(1-x-y)
$\mathbf{Eu_{0.033}Tb_{0.085}Gd_{0.882}L}$	0.03	0.07	0.90	0.033	0.085	0.882
$\mathbf{Eu_{0.013}Tb_{0.060}Gd_{0.927}L}$	0.01	0.045	0.945	0.013	0.060	0.927
$\mathbf{Eu_{0.0062}Tb_{0.0087}Gd_{0.9851}L}$	0.005	0.005	0.99	0.0062	0.0087	0.9851

Table S2. The parameters containing composition, temperature ranges (K), maximum relative sensitivity values (S_m, % K^{-1}), the temperature at which S_m is maximum (T_m, K) of several selected ratiometric luminescent MOF thermometers.

Luminescent M'LnMOF Thermometers	Temperature range (K)	S_m (% K^{-1})	T_m (K)	Ref.
$Eu_{0.0069}Tb_{0.9931}$-DMBDC	50 - 200	1.15	200	7d
$Tb_{0.9}Eu_{0.1}$-PIA	100 - 300	3.27	300	4a
$Tb_{0.98}Eu_{0.02}$-OA-DSTP	77 - 275	2.4	275	
$Tb_{0.98}Eu_{0.02}$-BDC-DSTP	77 - 225	2.8	225	21c
$Tb_{0.99}Eu_{0.01}$-BDC-DSTP	77 - 200	3.9	200	
$[Eu_{0.102}Tb_{0.898}(notpH_4)(NO_3)(H_2O)]\cdot 8H_2O$	18 - 300	3.9	38	21d
Tb 0.914 Eu 0.086 –PDA Tb 0.914 Eu 0.086 –PDA Tb 0.914 Eu 0.086 –PDA $Tb_{0.914}Eu_{0.086}$-PDA	10 - 325	5.96	25	21e
$Eu_{0.2}Tb_{0.8}L$		0.15		
$Eu_{0.1}Tb_{0.9}L$	40 - 300	0.11	300	22a
$Eu_{0.3}Tb_{0.7}L$		0.17		
$(Eu_1Tb_{99}$-HFA)@LA	197 - 287	1.107	287	22b
ZJU-88⊃perylene	293.15 – 353.15	1.28	193.15	22c
$Tb_{0.957}Eu_{0.043}$cpda	40 - 300	1.77	250	22d
d-U(600)-$Eu_{0.25}Tb_{0.75}(btfa)_3$(bpeta)	10 - 330	4.9	150	22e
$Tb_{0.99}Eu_{0.01}(BDC)_{1.5}\cdot(H2O)_2$	298 – 320	0.31	318	20b

$Eu_{0.0089}Tb_{0.9911}L$	**77-450**	**2.71**	**450**	**This work**
$Eu_{0.0066}Tb_{0.9934}L$	**77-450**	**3.76**	**450**	**This work**
$Eu_{0.033}Tb_{0.085}Gd_{0.882}L$	**77-450**	**3.62**	**400**	**This work**
$Eu_{0.013}Tb_{0.060}Gd_{0.927}L$	**77-450**	**6.11**	**430**	**This work**

DMBDC = 2,5-dimethoxy-1,4-benzenedicarboxylate, HPIA = 5-(pyridin-4-yl)isophthalic acid, H_2DSTP = 2,4-(2,2′:6′,2″-terpyridin-4′-yl)-benzenedisulfonic acid, OA = oxalic acid, BDC = 1,4-benzene dicarboxylic acid, notpH_6 = 1,4,7-triazacyclononane-1,4,7-triyl-tris(methylene-phosphonic acid), PDA = 1,4-phenylenediacetic acid, L = 1,3-bis(4-carboxyphenyl)imidazolium, cpda = 5-(4-carboxyphenyl)- 2,6-pyridinedicarboxylate, HFA = hexafluoroacetylacetone, ZJU-88 = $[Eu_2(QPTCA)(NO_3)_2(DMF)_4]\cdot(CH_3CH_2OH)_3$ (H_4QPTCA = 1,1′:4′,1″:4″,1‴-quaterphenyl-3,3‴, 5,5‴-tetracarboxylic acid), H_3cpda = 5-(4-carboxyphenyl)-2,6-pyridinedicarboxylic acid, bpeta = 1,2-bis(4-pyridyl)ethane.

Table S3. Crystal data and refinement results for **EuL**, **GdL** and **TbL**.

	EuL	**GdL**	**TbL**
Formula	$C_{23}H_{21}EuN_2O_{10}$	$C_{23}H_{21}GdN_2O_{10}$	$C_{23}H_{21}TbN_2O_{10}$
Formula weight	637.39	642.68	652.36
Crystal system	orthorhombic	orthorhombic	orthorhombic
space group	P*nma*	P*nma*	P*nma*
a (Å)	8.5023 (2)	8.5011 (3)	8.5052 (5)
b (Å)	17.3319 (4)	17.2958 (5)	17.3256 (4)
c (Å)	12.1180 (3)	12.0726 (3)	12.0864 (3)
α (°)	90	90	90
β (°)	90	90	90
γ (°)	90	90	90
Volume ($Å^3$)	1785.72 (7)	1775.08 (9)	1781.02 (7)
T (K)	100	100	100
Z	4	4	4
F (000)	1140	1144	1148
R_1 ($I>2\sigma(I)$)	0.0360	0.0467	0.0382
wR_2 (reflections)	0.1488	0.1064	0.1014
Goodness of fit on F^2	1.214	1.157	1.071

Table S4. Selected bond lengths (Å) and bond angles (°) for **EuL**, **GdL** and **TbL**.

Bond	Dist.	Bond	Dist.
Eu1—O6^{i}	2.355 (3)	Eu1—O4	2.450 (5)
Eu1—O6^{ii}	2.355 (3)	Eu1—O4^{v}	2.450 (5)
Eu1—O3^{iii}	2.394 (4)	Eu1—O2	2.465 (5)
Eu1—O3^{iv}	2.394 (4)	Eu1—O1	2.547 (4)
Angle	(º)	Angle	(º)
O6^{i}—Eu1—O6^{ii}	125.4 (2)	O4—Eu1—O4v	71.3 (2)
O6^{i}—Eu1—O3^{iii}	74.31 (14)	O6i—Eu1—O2	65.67 (11)
O6^{ii}—Eu1—O3^{iii}	137.57 (14)	O6ii—Eu1—O2	65.67 (11)
O6^{i}—Eu1—O3^{iv}	137.57 (14)	O3iii—Eu1—O2	137.92 (11)
O6^{ii}—Eu1—O3^{iv}	74.31 (14)	O3iv—Eu1—O2	137.92 (11)
O3^{iii}—Eu1—O3^{iv}	69.14 (18)	O4—Eu1—O2	109.38 (14)
O6^{i}—Eu1—O4	143.52 (14)	O4v—Eu1—O2	109.38 (14)
O6^{ii}—Eu1—O4	76.63 (14)	O6i—Eu1—O1	73.52 (10)
O3^{iii}—Eu1—O4	110.42 (12)	O6ii—Eu1—O1	73.52 (10)
O3^{iv}—Eu1—O4	71.80 (12)	O3iii—Eu1—O1	78.87 (11)
O6^{i}—Eu1—O4^{v}	76.63 (14)	O3iv—Eu1—O1	78.87 (11)
O6^{ii}—Eu1—O4^{v}	143.52 (14)	O4—Eu1—O1	142.66 (12)
O3^{iii}—Eu1—O4^{v}	71.80 (12)	O4v—Eu1—O1	142.66 (12)
O3^{iv}—Eu1—O4^{v}	110.42 (12)	O2—Eu1—O1	77.90 (16)

Symmetry codes: (i) 1-x, -1/2+y, 1-z; (ii) 1-x, 1-y, 1-z; (iii) x, 1/2-y, z; (iv) 1/2+x, y, 3/2-z; (v) 1/2+x, 1/2-y, 3/2-z.

Bond	Dist.	Bond	Dist.
Gd1—O6^{i}	2.322 (6)	Gd1—O3	2.425 (5)
Gd1—O6^{ii}	2.322 (6)	Gd1—O3^{v}	2.425 (5)
Gd1—O4^{iii}	2.367 (6)	Gd1—O1	2.465 (10)
Gd1—O4^{iv}	2.367 (6)	Gd1—O2	2.517 (6)
Angle	(º)	Angle	(º)
O6^{i}—Gd1—O6^{ii}	123.0 (4)	O3—Gd1—O3^{v}	71.5 (2)
O6^{i}—Gd1—O4^{iii}	138.8 (2)	O6^{i}—Gd1—O1	64.3 (2)
O6^{ii}—Gd1—O4^{iii}	75.5 (3)	O6^{ii}—Gd1—O1	64.3 (2)
O6^{i}—Gd1—O4^{iv}	75.5 (3)	O4^{iii}—Gd1—O1	137.7 (2)
O6^{ii}—Gd1—O4^{iv}	138.8 (2)	O4^{iv}—Gd1—O1	137.7 (2)
O4^{iii}—Gd1—O4^{iv}	69.6 (3)	O3—Gd1—O1	108.7 (2)
O6^{i}—Gd1—O3	143.2 (2)	O3^{v}—Gd1—O1	108.7 (2)
O6^{ii}—Gd1—O3	76.9 (2)	O6^{i}—Gd1—O2	73.72 (16)
O4^{iii}—Gd1—O3	72.21 (19)	O6^{ii}—Gd1—O2	73.72 (16)
O4^{iv}—Gd1—O3	111.2 (2)	O4^{iii}—Gd1—O2	78.32 (18)
O6^{i}—Gd1—O3^{v}	76.9 (2)	O4^{iv}—Gd1—O2	78.32 (18)
O6ii—Gd1—O3v	143.2 (2)	O3—Gd1—O2	142.59 (13)
O4iii—Gd1—O3v	111.2 (2)	O3v—Gd1—O2	142.59 (13)

O4iv—Gd1—O3v	72.21 (19)	O1—Gd1—O2	78.6 (3)

Symmetry codes: (i) 1-x, -1/2+y, 1-z; (ii) 1-x, 1-y, 1-z; (iii) x, 1/2-y, z; (iv) 1/2+x, y, 3/2-z; (v) 1/2+x, 1/2-y, 3/2-z.

Bond	Dist.	Bond	Dist.
Tb1—O6^{i}	2.339 (4)	Tb1—O3^{iv}	2.434 (4)
Tb1—O6^{ii}	2.339 (4)	Tb1—O3^{v}	2.434 (4)
Tb1—O4	2.366 (4)	Tb1—O1	2.462 (7)
Tb1—O4^{iii}	2.366 (4)	Tb1—O2	2.522 (5)
Angle	**(º)**	**Angle**	**(º)**
O6^{i}—Tb1—O6^{ii}	123.5 (3)	O3^{iv}—Tb1—O3^{v}	71.55 (19)
O6^{i}—Tb1—O4	138.66 (16)	O6^{i}—Tb1—O1	64.64 (14)
O6^{ii}—Tb1—O4	75.04 (17)	O6^{ii}—Tb1—O1	64.64 (14)
O6^{i}—Tb1—O4^{iii}	75.04 (17)	O4—Tb1—O1	137.75 (13)
O6^{ii}—Tb1—O4^{iii}	138.66 (16)	O4^{iii}—Tb1—O1	137.75 (13)
O4—Tb1—O4^{iii}	69.9 (2)	O3^{iv}—Tb1—O1	108.31 (16)
O6^{i}—Tb1—O3^{iv}	143.11 (14)	O3^{v}—Tb1—O1	108.31 (16)
O6^{ii}—Tb1—O3^{iv}	76.68 (14)	O6^{i}—Tb1—O2	73.61 (11)
O4—Tb1—O3^{iv}	72.33 (13)	O6^{ii}—Tb1—O2	73.61 (11)
O4^{iii}—Tb1—O3^{iv}	111.46 (13)	O4—Tb1—O2	78.59 (12)
O6^{i}—Tb1—O3^{v}	76.68 (14)	O4^{iii}—Tb1—O2	78.59 (12)
O6^{ii}—Tb1—O3^{v}	143.11 (14)	O3^{iv}—Tb1—O2	142.72 (10)
O4—Tb1—O3^{v}	111.46 (13)	O3^{v}—Tb1—O2	142.72 (10)
O4^{iii}—Tb1—O3^{v}	72.33 (13)	O1—Tb1—O2	78.5 (2)

Symmetry codes: (i) 1-x, -1/2+y, 1-z; (ii) 1-x, 1-y, 1-z; (iii) x, 1/2-y, z; (iv) 1/2+x, y, 3/2-z; (v) 1/2+x, 1/2-y, 3/2-z.